

B mesons as novel probes of QGP

João Gonçalves^{1,a} and Alexandra Pardal^{2,b}

¹*Instituto Superior Técnico, Lisboa, Portugal*

²*Faculdade de Ciências, Lisboa, Portugal*

Project supervisors: N. Leonardo, J. Silva

October 2019

Abstract. In this work we study B mesons as novel probes of the quark gluon plasma (QGP). We used PbPb data collected by the CMS experiment at the LHC in November 2018. The B^+ and B_s production differential cross-sections in PbPb collisions are measured. The cross sections of the two mesons and their ratios provide unique information about the properties of the QGP and how the hot and dense QCD medium affects the hadronization of the b quark. The B_s meson is observed for the first time in heavy ion collisions.

KEYWORDS: LHC, QGP, heavy flavour, production cross section, quark fragmentation, strangeness enhancement

Contents

1	Introduction	1
2	The CMS detector	1
3	Data, MC samples and signal selection	2
4	Extracting signals from busy ion collisions	2
4.1	Sideband subtraction	2
4.2	sPlot	3
5	Yield measurement	4
5.1	Likelihood model	4
5.2	Yield results and significance	4
5.3	Fit validation	5
5.4	Systematic uncertainties from fit procedure	5
5.5	Systematic uncertainties from PDF modeling	6
5.6	Differential yield	6
6	Efficiency determination	6
7	Differential cross-section measurement	7
7.1	Data representation (abscissae)	7
7.2	Systematic uncertainties	8
8	Skills acquired	8
9	Summary and perspectives	8

1 Introduction

Quantum chromodynamics (QCD) predicts that under extreme conditions of temperature and/or density the Quark-Gluon Plasma (QGP) is formed. The QGP existed microseconds after the Big Bang and it is a state of matter formed by deconfined quarks and gluons. It can be recreated at the LHC by colliding heavy nuclei (Pb) at the highest energies [1].

B mesons are composed by a bottom antiquark (\bar{b}) and an up, down, strange or charm quark. In this experimental

work we study the B^+ meson ($\bar{b}u$) and the B_s meson ($\bar{b}s$) [2]. Bottom quarks are created in the initial hard scattering stage and retain their identity while traversing the medium they are in, thus recording information about its evolution. By comparing pp collisions (vacuum medium) with PbPb collisions (QGP), we can therefore use B mesons as probes to study the QGP properties. The goal of this study is to measure the B meson's cross section in PbPb collisions at 5 TeV and to study how the QGP affects the hadronization of the b quark.

The cross-section is given by:

$$\sigma = \frac{N}{\varepsilon \mathcal{A} \mathcal{B} \mathcal{L}} \quad , \quad (1)$$

where N is the signal yield, \mathcal{L} the luminosity, \mathcal{B} the branching fraction, \mathcal{A} the acceptance and ε the efficiency. While N is measured from data, through the implementation of an unbinned fitting procedure in Section 5.1, ε and \mathcal{A} are determined from Monte Carlo (MC) simulation, that is validated through the methods of sideband subtraction and sPlot, in Section 4.

2 The CMS detector

The Compact Muon Solenoid (CMS) is one of the four large experiments at the Large Hadron Collider (LHC). Fig. 1 represents a transversal slice of the detector and its layers. When the particles travel through the detector they leave signatures (deposits of energy) in different layers, which allows their identification. In Fig. 1 it is possible to identify these layers from inward to outward: the silicon tracker, which measures the positions of passing charged particles allowing their track reconstruction; the electromagnetic calorimeter (ECAL) and the hadronic calorimeter (HCAL), which measure the energy of particles; the solenoid, with a magnetic field of 3.8 T, that bends the trajectory of particles, allowing the measurement of their charge and momentum; and the muon chambers, where the muons are detected, since they are able to penetrate dense materials. The most important subdetectors for this analysis are the silicon tracker and muon

^ae-mail: joaofranciscogoncalves@tecnico.ulisboa.pt

^be-mail: alexandrampardal@gmail.com

detectors, that are employed to trigger and measure the final states here explored: muons (tracker+muon chamber) and charged hadrons (tracker). A detailed description of the CMS detector can be found in Ref. [3].

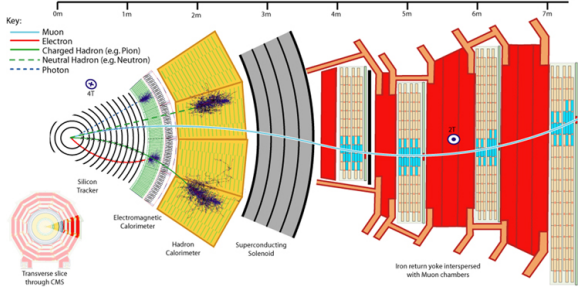


Figure 1. Schematic transverse view of the CMS detector.

3 Data, MC samples and signal selection

The decay channels used in the analysis are:

- $B^+ \rightarrow J/\psi K^+$ with $J/\psi \rightarrow \mu^+ \mu^-$,
- $B_s^0 \rightarrow J/\psi \phi$ with $J/\psi \rightarrow \mu^+ \mu^-$, $\phi \rightarrow K^+ K^-$

This analysis is performed using the 2018 PbPb data at $\sqrt{s_{NN}}=5.02$ TeV, which has an integrated luminosity of 1.5 nb^{-1} . The analysis uses the dimuon primary datasets (DoubleMu PD). Events used in the study were collected with a trigger requiring the presence of two muon candidates. No explicit kinematic selection is applied online, either on (transverse) momentum or pseudo-rapidity.

Dedicated PbPb B meson signal samples were generated by PYTHIA8 tune CUETPM8 [4]. The mesons are forced to follow the intended signal decay chains, by means of the EVTGEN package. The B phase space is restricted to $p_T > 5.0$ GeV and $|\eta| < 2.4$. Final state radiation (FSR) is generated using PHOTOS. The selected signal B PYTHIA8 events were embedded into a PbPb background simulated with HYDJET [5].

The main variables employed in the event selection and that are studied in this analysis are the following: α , angle between B meson displacement and its momentum; $trk\eta$, pseudorapidity of the K track ($\eta = -\ln(\tan \theta/2)$, where θ is the polar angle of the trajectory of a particle with respect to the counterclockwise proton beam); $mu\eta$, pseudorapidity of the muons; p_T , B meson transverse momentum; $trkp_T$, transverse momentum of the K track; $mu p_T$, transverse momentum of the muons; y , B meson rapidity; $trky$: rapidity of the K track.

Instead of applying selection criteria separately to each signal-vs-background discriminating variable, a Boosted Decision Tree (BDT) method is employed, combining all variables. A BDT is a group of decision trees trained sequentially, each placing different requirements on the variables, to achieve the best classification of events. The training uses samples of signal MC and background events from mass sidebands. The BDT combines all the input variables and allows us to optimally distinguish between signal and background.

The selection is separately optimized for each meson. The selection variables and procedure do not involve the B meson's invariant mass, M ; instead, this variable will be used in the fits performed to the data.

4 Extracting signals from busy ion collisions

This section presents the techniques employed for extracting signal distributions from data. The methods are employed throughout the following sections.

4.1 Sideband subtraction

The sideband subtraction is a method that allows us to obtain the signal distribution of a given variable of interest directly from data, by removing the background. This method relies on the use of the invariant mass of the reconstructed candidates as a separation variable, which we assume in turn to be independent from all other variables to be studied.

In the invariant mass plot we can distinguish two regions: the peak zone, which contains both signal and background, and the sideband zones, which contains background only. To obtain the signal distribution V_{signal} for the variable of interest V , we start with its distribution in the peak zone, V_{peak} and subtract the distribution V_{sideband} obtained from the sideband zone:

$$V_{\text{signal}} = V_{\text{peak}} - \alpha \cdot V_{\text{sideband}} . \quad (2)$$

The subtraction parameter α reflects the relative background yield in the signal and background regions:

$$\alpha = \frac{P}{L + R} . \quad (3)$$

To determine it, we fit the data sideband region with a suitable background model, and integrate the obtained background fit function over the peak zone, yielding value P , and over the sideband zones, yielding L and R (for left and right sideband). This is illustrated in Fig. 2.

The sideband zones contain only combinatorial-like background that can be extrapolated from the sideband to the signal region, which is true in the case of the B_s meson but not so for the B^+ meson. While this assumption holds for the B_s , in the case of the B^+ the left sideband cannot be used. This is because the B^+ left sideband, in addition to background of the combinatorial type, also contains contributions from partially reconstructed B decays (e.g. $B \rightarrow hX$, where h is a charged hadron and X stands for additional decay products). Since this type of background is absent from the peak zone, it must not be subtracted. We thus do not consider the left sideband in this case, and the background fit to the data is performed only on the right sideband zone, and Eq. 3 is used with $L = 0$.

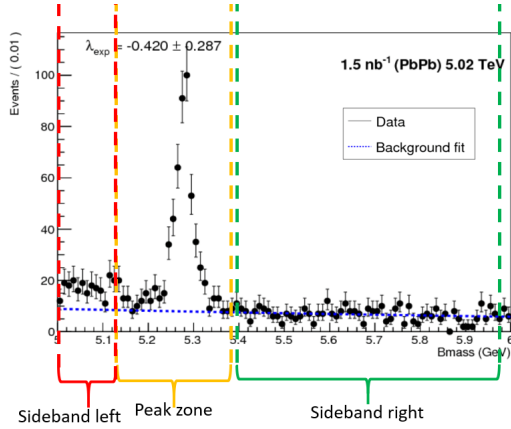


Figure 2. Illustration of the three relevant regions in the invariant mass spectrum. As specified in the text, the left sideband cannot be employed for the B^+ case.

In Figs.3-4 examples of the results are presented. The first plot shows the total data, the signal distribution (obtained by removing the background from the data) and the background (obtained from the fit) for one of the variables in study. The second plot shows the signal data in comparison to the MC simulation, and their ratio.

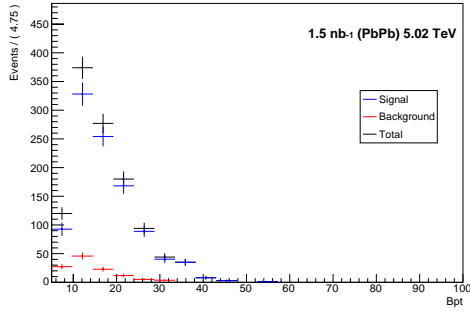


Figure 3. Sideband subtraction results for B^+ meson's p_T .

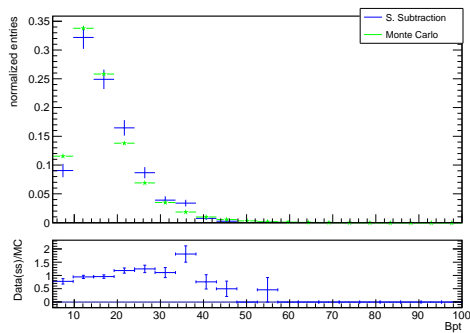


Figure 4. Sideband subtraction results for B^+ meson's p_T and comparison to MC simulation. The lower panel shows their ratio.

4.2 sPlot

The sPlot method [6] is likelihood based. In order to use it we first need to fit the data using a discriminating variable, namely the B^+ meson candidates' invariant mass. This method, like the one described in the previous section, assumes the discriminating variable chosen to be independent from the variables we wish to study. We then use the

fit to attribute to each event two weights: w_s , which corresponds to the probability of it belonging to the signal, and w_b , which corresponds to the probability of it belonging to the background. The weights are qualitatively represented in Fig. 5.

The signal distributions are obtained by projecting the data using the signal weights. The mass fitting is explained in section 5.1.

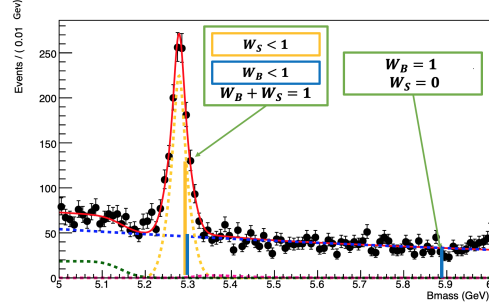


Figure 5. Representation of the sPlot weights, overlaid on the fit projection of B^+ candidates invariant mass.

In Figs.6-9 the results are presented. The plots displayed first show the signal distribution and the background for some of the variables in study. The plots displayed after show the signal data in comparison to the MC simulation. The distributions are normalized to the same unit area.

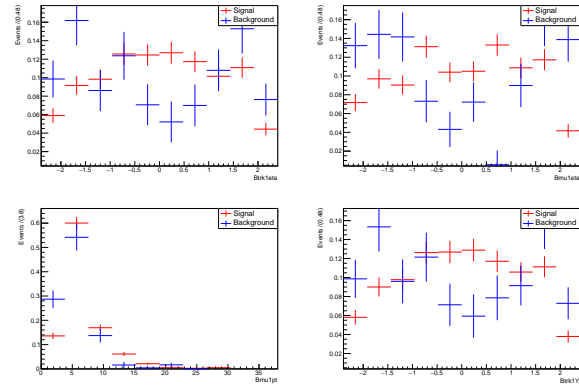


Figure 6. sPlot results for B^+ meson's $trk\eta$, $mu\eta$, $mu p_T$ and $trk y$.

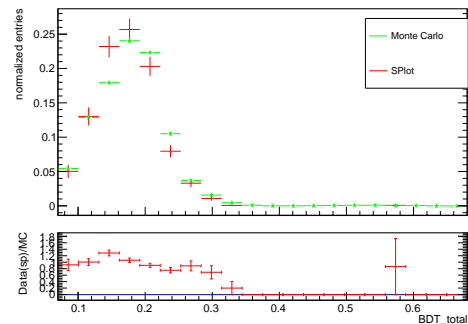


Figure 7. sPlot results vs MC for B^+ meson's BDT and ratio.

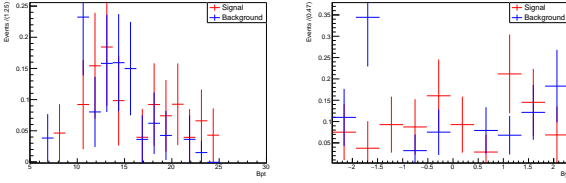


Figure 8. sPlot results for B_s meson's p_T and y .

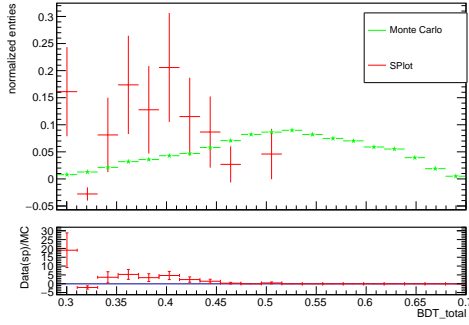


Figure 9. Sideband subtraction results vs MC for B_s meson's BDT .

For the B_s meson there are relatively less events available, but the data and MC are consistent within the error bars. In Figs. 7 and 9, the higher bins are not sufficiently populated in data. For those bins, the ratio was taken as 1. The ratios will later be used to quantify the discrepancies between data and MC. In Fig.10 an example comparing the two methods and the Monte-Carlo simulation is presented.

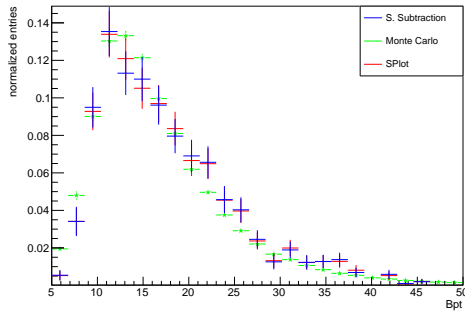


Figure 10. Sideband subtraction results vs MC vs sPlot for B_+ meson's p_T .

Both methods return compatible results. Nevertheless, the sPlot is a more robust method since it uses information from a full likelihood fit and so it was the method chosen to calculate the ratios used in the efficiency systematic error.

5 Yield measurement

In this section the procedure for extracting the signal yield (N) values and uncertainties is presented.

5.1 Likelihood model

The B mesons' invariant mass spectra is fitted using an extended unbinned maximum likelihood (EUML) fit. The EUML fit is implemented using the RooFit package [7]. The likelihood function \mathcal{L} is given by:

$$\mathcal{L}(\vec{\lambda}|\{m_i\}) = \left(\prod_{i=1}^{N_{\text{obs}}} \sum_{\alpha} N_{\alpha} \mathcal{P}_{\alpha}(m_i|\vec{\lambda}) \right) \times \frac{e^{-N} N^{N_{\text{obs}}}}{N_{\text{obs}}!}. \quad (4)$$

The B meson signal component is modeled by a sum of two Gaussian functions with same mean:

$$\mathcal{P}_S(m|\mu_1, \sigma_1, \mu, \sigma_2) = f \cdot \text{Gauss}(m; \mu, \sigma_1) + (1 - f) \cdot \text{Gauss}(m; \mu_2, \sigma_2). \quad (5)$$

The combinatorial background is described by an exponential function.

In the case of the B^+ , there are additional background components: (i) partially reconstructed B meson decays (e.g. $B_s^0 \rightarrow J/\psi K^+ K^-$ where one kaon is missed), and (ii) the Cabibbo-suppressed decay $B^+ \rightarrow J/\psi \pi^+$. The former results in a threshold structure to the left of the spectrum, and is described by a complementary error function, while the latter is described with a shape (and normalization relative to signal) obtained from simulation.

The combined PDF expressions for the B^+ meson candidates is given by:

$$L(m) = N_S (\alpha \cdot G(\sigma_1, \mu) + (1 - \alpha) \cdot G(\sigma_2, \mu)) + N_{CB}(\text{Exp}(\lambda)) + N_{erf}(\text{Erf}(sh, sc)) + N_{j\psi\text{fixed}}. \quad (6)$$

and for the B_s meson candidates by:

$$L(m) = N_S (\alpha \cdot G(\sigma_1, \mu) + (1 - \alpha) \cdot G(\sigma_2, \mu)) + N_{CB}(\text{Exp}(\lambda)). \quad (7)$$

5.2 Yield results and significance

The fits to the full datasets are shown in Figs. 11 and 12, for B^+ and B_s , respectively.

The signal yields, along with their statistical uncertainties, are extracted directly as parameters from the fit. The figures display also the values of all floating parameters, $\vec{\lambda}$.

When carrying out differential measurements, the fit procedure is applied to the invariant mass spectra of data subsets (e.g. p_T bins).

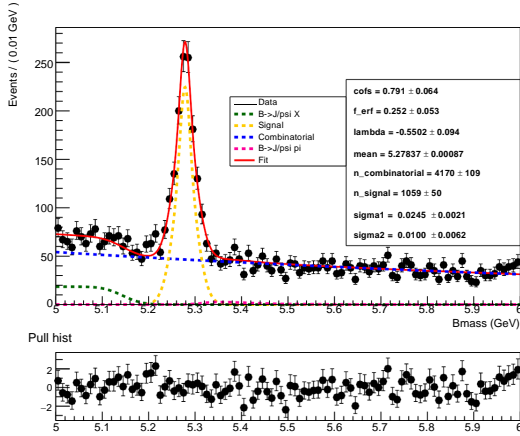


Figure 11. Fit to the invariant mass of the B^+ candidates (full sample). The fit results, with signal and background component projections, are overlaid to the data. The bottom panel displays the pulls between data and fit function.

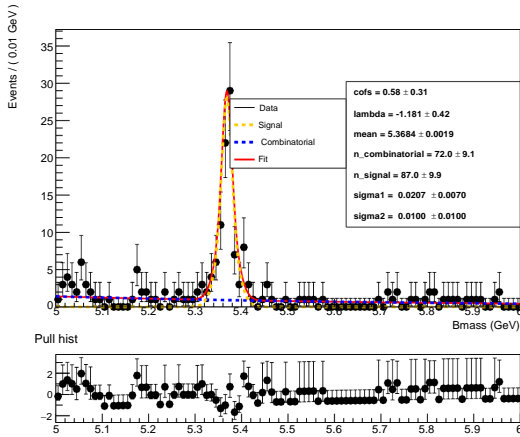


Figure 12. Fit to the invariant mass of the B_s candidates (full sample). The fit results, with signal and background component projections, are overlaid to the data. The bottom panel displays the pulls between data and fit function.

The significance can be estimated by the quotient between the signal yield and its uncertainty:

$$\begin{aligned}
 B^+ &: N/\sigma_N = 29, \\
 B_s &: N/\sigma_N = 8.8.
 \end{aligned}$$

5.3 Fit validation

It is important to validate the fit implementation, to verify it returns the correct estimated parameters and checking its consistency. To do that, the RooFit class `RoomCStudy` is employed to generate pseudo-experiments, also referred to as "toy MC", that is, candidate (mass) distributions sampled from the original PDF, with the parameters $\vec{\lambda}$ obtained

from fitting the data. For each meson, 5000 toy MCs are generated.

The distributions for the fitted signal yield of the toy MCs are expected to follow a Gaussian curve centered on the value obtained from the original fit to the data, and used to generate the toy MC. The pull distribution obtained from the fits to the toy MCs is itself expected to follow a unit Gaussian (centered at 0 and with sigma equal to 1). The possible deviations will be used to derive the associated systematic uncertainty.

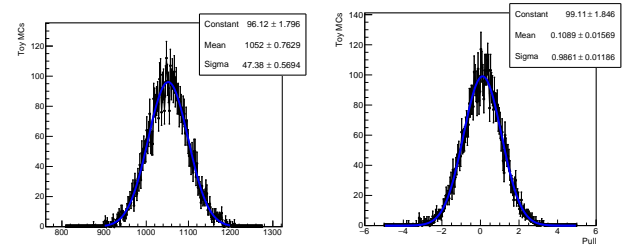


Figure 13. Distribution for the B^+ fitted signal yield (left) and pull width (right).

5.4 Systematic uncertainties from fit procedure

Tables 1 and 2 show the results for the B^+ meson and the B_s meson obtained in the last section. The pull mean and pull sigma for each meson were close to expectation, validating the fit. The small deviations are nevertheless used to estimated systematic uncertainties related to the fit implementation and possible fit biases. These can be estimated in two ways: from the signal yield distribution or from its pull, as obtained from the toy MC study (PDF modelling).

In order to obtain the systematic uncertainty from the signal yield distribution, we subtract the parameter distribution mean given by the toy MCs from the input signal yield used to generate the toys. To evaluate the systematic uncertainty from the pull distribution mean we multiply it by the signal yield sigma given by the fit.

In order to evaluate the relative uncertainties, the value for absolute systematic uncertainty is divided by the signal yield returned by the fit. The two methods yield compatible systematic estimates, found to be smaller than 2%.

Table 1. Fit validation results for B^+ .

	Pull mean	Sgn yield mean	Pull width
Exp. value	0	1059	38
Value	0.109±0.016	1052±1	47.38±1
Dev.	0.109	7	-9.38
Syst uncertainty	5.445	7	-9.38
Rel uncertainty	0.514%	0.661%	24.684%

Table 2. Fit validation results for B_s .

	Pull mean	Sgn yield mean	Pull width
Exp. value	0	87	9.9
Value	-0.168±0.017	85.7±0.2	10.69±0.1
Dev.	0.168	1.34	0.79
Syst uncertainty	-1.663	1.34	0.79
Rel uncertainty	1.971%	1.540%	7.98%

5.5 Systematic uncertainties from PDF modeling

Systematic uncertainties on the signal yield measurement may arise, besides potential intrinsic fit biases, from PDF component modeling. The following variations are implemented:

- signal PDF: one Gaussian (instead of two);
- background PDF: first order polynomial (instead of an exponential);
- fitting range: exclude the left sideband region from the fit.

The systematic error is obtained by summing in quadrature the yield differences obtained with the above variations: $\sigma_{\text{syst}} = \sqrt{\sigma_{\text{signal-pdf}}^2 + \sigma_{\text{bkg-pdf}}^2 + \sigma_{\text{fit-range}}^2}$.

The p_T -differential yields, with statistical and systematic uncertainties are shown in Tables 3 and 4 and Figs. 14 and 15, for B^+ and B_s , respectively. The systematic uncertainty values shown are absolute errors.

5.6 Differential yield

In addition to the fits to the full data sets shown in Fig. 11 and 12, the fits have been performed in addition in p_T -ranges.

The p_T -differential yields, with statistical and systematic uncertainties are shown in Tables 3 and 4 and Figures 14 and 15, for B^+ and B_s respectively. The systematic uncertainty values shown are absolute errors.

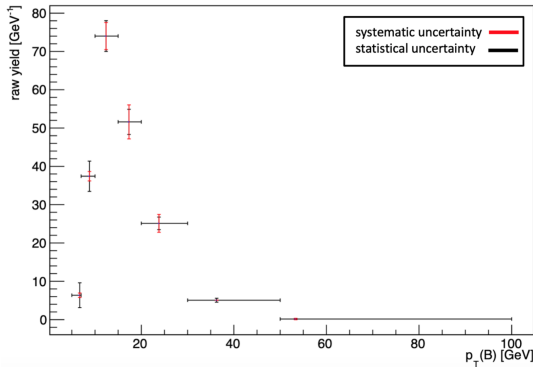


Figure 14. Differential yield as function of p_T for B^+ . The statistical (systematic) uncertainty is shown by the vertical black (red) lines. The horizontal lines denote the p_T bin ranges, while the point abscissae are given by the bin-average signal p_T .

Table 3. Signal yield normalized by bin width, with statistical and systematic uncertainties from PDF modeling for B^+ meson.

p_T (GeV)	dN_{signal}/dp_T	σ_{stat}	σ_{syst}
5-7	6.358	3.240	0.574
7-10	37.412	3.961	1.232
10-15	74.012	4.014	3.546
15-20	51.606	3.283	4.431
20-30	25.117	1.637	2.332
30-50	5.062	0.507	0.032
50-100	0.153	0.054	0.186

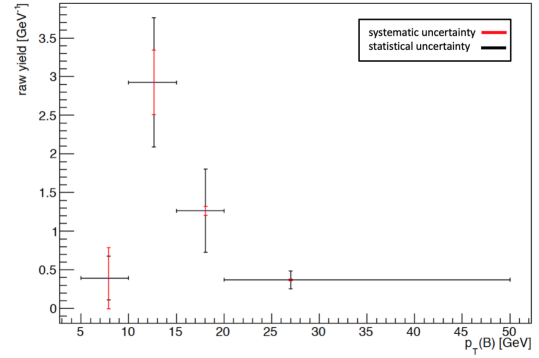


Figure 15. Differential yield as function of p_T for B_s . The statistical (systematic) uncertainty is shown by the vertical black (red) lines. The horizontal lines denote the p_T bin ranges, while the point abscissae are given by the bin-average signal p_T .

Table 4. Signal yield normalized by bin width, with statistical and systematic uncertainties from PDF modeling for B_s meson.

p_T (GeV)	dN_{signal}/dp_T	σ_{stat}	σ_{syst}
5-10	0.392	0.283	0.395
10-15	2.924	0.836	0.417
15-20	1.264	0.539	0.057
20-50	0.371	0.115	0.012

6 Efficiency determination

The efficiency measures the amount of lost signal and it is given by:

$$\epsilon = \frac{N_{\text{after cuts}}}{N_{\text{before cuts}}} \quad (8)$$

The efficiency is determined from MC simulation. Potential discrepancies between data and simulation reflect as an uncertainty in the efficiency calculation. Specifically, the efficiency systematic uncertainty is given by:

$$\Delta = \frac{\epsilon^1 - \epsilon^0}{\epsilon^0}, \quad (9)$$

where ϵ^0 is the nominal efficiency (i.e., calculated with the nominal MC) and ϵ^1 is the efficiency calculated with re-weighted MC, where the weights quantify the data-MC disagreement.

In order to determine the value of ϵ^1 it is necessary to evaluate the MC-correcting weights. These are obtained from comparing distributions of data and MC, for variables employed in the selection. Specifically, the weights correspond to the ratio between the data and the MC distributions (see Section 4.2).

The selection was optimized using a multivariable technique that employs the BDT. It was therefore this variable, the BDT score, that was employed for the calculation of the efficiency's systematic uncertainty. The optimization was done separately per p_T -bin – as background level and characterization may be expected to depend strongly on p_T , such splitting should result in an improved optimization. The total BDT histogram is constructed as follows: for each candidate, the appropriate BDT score is

retrieved based on its p_T value; it is this BDT score that is histogrammed and processed (with sPlot).

The systematic uncertainties of the efficiency are presented in Figs. 17 and 16 and Table 5.

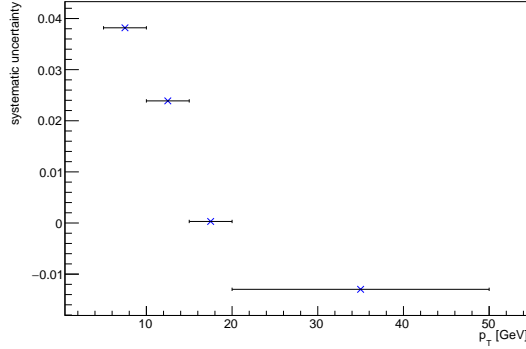


Figure 16. Efficiency's systematic uncertainty for B^+ meson.

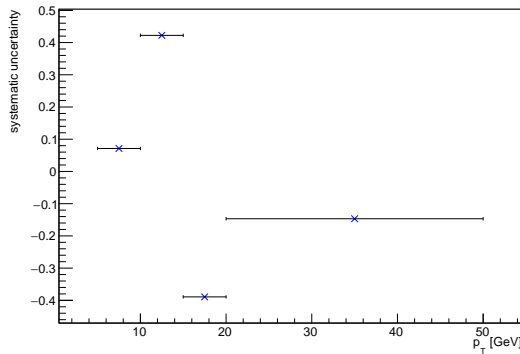


Figure 17. Efficiency's systematic uncertainty for B_s meson.

Table 5. Efficiency's systematic uncertainties.

p_T (GeV)	$B^+ \sigma_{syst}$	$B_s \sigma_{syst}$
5-10	0.0382	0.071
10-15	0.0239	0.422
15-20	0.0003	-0.389
20-50	-0.0130	-0.147
5-50	0.0382	-0.123

The systematic errors are noticeably larger for the B_s meson. This is because for this meson there are less candidates in data, which introduces a bigger statistical component in the systematics evaluation.

7 Differential cross-section measurement

Using Equation (1), the results obtained for the normalized cross-sections of the B^+ and B_s mesons are shown in Figs. 18 and 19. The statistical and systematic uncertainties, represented in the figures as black and red bars, respectively, are summarized in Tables 6 and 7.

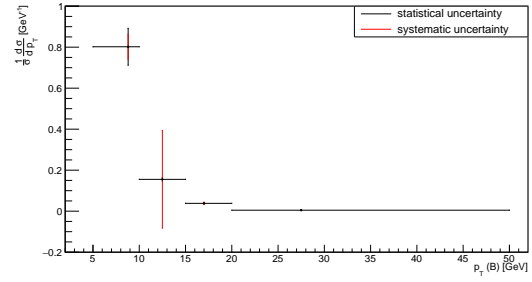


Figure 18. Normalized B^+ meson differential cross-section as function of p_T .

Table 6. Systematic and statistical relative uncertainties of the B^+ cross section measurement vs p_T .

p_T (GeV)	σ_{syst}	σ_{stat}
5-10	0.07	0.11
10-15	1.53	0.05
15-20	0.16	0.06
20-50	0.08	0.05

For the B_s meson the results are presented in Fig.19 and Table 7.

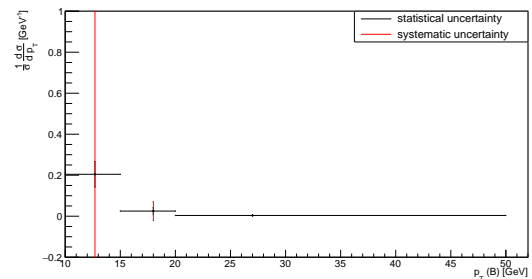


Figure 19. Normalized B_s meson differential cross-section as function of p_T .

Table 7. Systematic and statistical relative uncertainties of the B_s cross section measurement vs p_T .

p_T (GeV)	σ_{syst}	σ_{stat}
10-15	2.55	0.29
15-20	0.52	0.43
20-50	0.16	0.31

7.1 Data representation (abscissae)

In a (p_T -)differential measurement, the signal yields (N_{signal}) are determined for each (p_T) bin. The values of p_T are given by the bin average. In order to evaluate it, the data subset per bin is selected, fitted and the floating parameters (including the N_{signal}) are saved. The p_T value for the bin is determined as the weighted average, using the signal weights (w_s) obtained from sPlot (Section 4.2).

7.2 Systematic uncertainties

The PbPb sample corresponds to an integrated luminosity of $(1.50 \pm 0.015) \times 10^{-9} b^{-1}$. The uncertainty is propagated as systematic uncertainty in the cross section measurement.

The branching fractions of the B_s and B^+ decay chains and their systematic uncertainties were calculated based on the values presented in the Particle Data Group (PDG) [8] and are summarized in Table 8.

Table 8. Branching fractions and their uncertainties.

Decay	Branching fraction
$B^+ \rightarrow J/\psi K^+$	$(1.01 \pm 0.03) \times 10^{-3}$
$J/\psi \rightarrow \mu^+ \mu^-$	$(5.93 \pm 0.06) \times 10^{-2}$
$B_s^0 \rightarrow J/\psi \phi$	$(1.08 \pm 0.08) \times 10^{-3}$
$\phi \rightarrow K^+ K^-$	$(4.89 \pm 0.01) \times 10^{-1}$
$B^+ \rightarrow J/\psi K^+ \rightarrow \mu^+ \mu^-$	$(5.99 \pm 0.23) \times 10^{-2}$
$B_s^0 \rightarrow J/\psi \phi \rightarrow \mu^+ \mu^- K^+ K^-$	$(3.13 \pm 0.30) \times 10^{-5}$

8 Skills acquired

Through this work, we strengthened our programming skills with C++ and ROOT. We learned how to extract signal information from data using unbinned fitting and background subtraction procedures. We became familiar with how to perform a measurement with LHC data, including extracting physics results and the evaluation of its systematic uncertainties. We became actively involved in an ongoing CMS analysis and learned about the process of taking part in research at a large scientific collaboration.

9 Summary and perspectives

We have explored B mesons as novel probes of the QGP with CMS. A detailed study of MC validation was performed by extracting signal from data using the sideband-subtraction and sPlot methods. From the results obtained we concluded that the Monte-Carlo reasonably described the data. The leftover discrepancy was accounted for by calculating the efficiency's systematic error.

The differential production cross-section of B^+ and B_s mesons in PbPb collisions at 5.02 TeV was measured and its systematic uncertainties were all evaluated. For the B^+ meson, the dominant uncertainties are due to discrepancies between the data and MC, while for the B_s meson the results are affected mainly by the reduced statistics.

In the future, additional LHC PbPb data, to be collected in upcoming runs, will allow a more precise measurement of the B meson properties and how these are affected by the QGP. Repeating the analysis with pp data will further allow the determination of the QGP medium effects and properties.

Acknowledgements

We thank our supervisors and the organization of the LIP summer student program. During our internship we had the opportunity of becoming involved and contributing to an ongoing CMS analysis [9], developed by the LIP and MIT groups. We are grateful for having been welcomed as analysis members, and thank discussions and comments received during the development of our work.

References

- [1] X. Dong, Y.J. Lee, R. Rapp (2019), 1903.07709
- [2] A.M. Sirunyan et al. (CMS), Phys. Lett. **B796**, 168 (2019), 1810.03022
- [3] CMS Collaboration, Journal of Instrumentation **3**, S08004 (2008), The CMS experiment
- [4] T. Sjöstrand, S. Ask, J.R. Christiansen, R. Corke, N. Desai, P. Ilten, S. Mrenna, S. Prestel, C.O. Rasmussen, P.Z. Skands, Comput. Phys. Commun. **191**, 159 (2015), 1410.3012
- [5] A.M. Sirunyan et al. (CMS), Phys. Lett. **B796**, 168 (2019), and references therein, 1810.03022
- [6] M. Pivk, F.R.L. Diberder, Nucl. Instrum. Meth. A 555 356 (2005), RooStats::SPlot Class Reference
- [7] R. Brun, F. Rademakers, Proceedings AIHENP'96 Workshop, Lausanne, Sep. 1996, Nucl. Inst. Meth. in Phys. Res. A 389 pp. 81–86 (1997), see also <http://root.cern.ch/>
- [8] Particle Data Group, Phys. Rev. D **98**, 030001 (2018)
- [9] A. Pardal, J. Gonçalves, J. Silva, N. Leonardo (2019), CMS AN-2019/219